—Technical Note—

RAREFACTION EFFECT ON GAS FLOW IN MICROCHANNELS WITH VARIOUS ASPECT RATIOS

C.-Y. Huang * **J.-S. Li**

Department of Power Mechanical Engineering
National Tsing Hua University
Hsinchu, Taiwan

ABSTRACT

This study investigated the effect of rarefaction on microchannel gas flow by measuring pressure profiles in microchannels with various aspect ratios. Pressure-sensitive paint (PSP) was applied in rectangular microchannels to obtain the global flow field by using detailed pressure data. The effect of rarefaction on the microchannel gas flow was clearly observed in the microchannels through the pressure data obtained using PSP measurements. A nonlinear pressure distribution was observed inside the microchannels, and this distribution decreased as the Knudsen number (Kn) increased because of the rarefaction effect. The dimensionless pressure deviation from the linear assumption dropped from 0.25 to 0 when the outlet Kn number increased to 0.066 in the 100-μm-wide microchannel, and the dimensionless location of the maximum deviation moved upstream because of the gaseous slip at the wall. The nonlinear pressure distribution also decreased in the 50-μm-wide microchannel as the outlet Kn number increased; however, the peak of the maximum deviation could no longer be identified because of the characteristic of the narrow channel.

Keywords: Gas flow, Microchannel, Pressure-sensitive paint (PSP), Rarefaction effect.

1. INTRODUCTION

Researchers have extensively investigated the flow fields in microdevices for decades. A straight microchannel flow, which is used to deliver fluids in many microdevices, is a classic problem in microfluidics. The physics of a microchannel flow, which deviate from that of a macroscale channel flow, demonstrate a nonlinear pressure distribution engendered by compressibility effects in small channels. However, such a nonlinear pressure distribution decreases if the effect of rarefaction starts dominating the flow field. Efforts have been exerted to understanding the effect of rarefaction, which can be further applied to micro/nanoscale gas delivery.

To investigate the physical phenomena of microchannel gas flow, different approaches such as experimental methods, numerical simulation, and theoretical analysis have been applied. Pong *et al*. fabricated microsize pressure transducers and embedded them next to a microchannel to measure the pressure distribution. They reported that the compressibility effect in the microchannel flow engendered nonlinear pressure distributions [1]. Arkilic *et al*. calculated pressure and velocity variations inside a two-dimensional (2D) straight microchannel by using Navier-Stokes equations with a first-order slip boundary condition [2]. They observed a slip flow at the boundary, which resulted in an increase in the mass flow rate. Hsieh *et al*. analyzed the pressure variation in a straight microchannel by using nitrogen gas [3]. They placed pressure sensors at the microchannel inlet and exit to obtain pressure data and used a 2D analytical solution to interpolate the pressure distribution inside the microchannel. A Knudsen number (Kn) increasing to 0.01 can be considered to represent a slip flow condition, which reduces the friction factor and effect of nonlinear pressure distribution.

When the characteristic length of a microchannel decreases, the flow regime changes from a continuum flow, slip flow, and transition flow to a free molecular flow [4]. The difference in flow regimes can be calculated using Kn number, which is defined as follows:

$$\mathrm{Kn} = \frac{\lambda}{\mathrm{L}} \tag{1}$$

where L is the characteristic length of the microchannel and λ is the mean free path of gas molecules.

* Corresponding author (cyhuang@pme.nthu.edu.tw)

DOI : 10.1017/jmech.2016.62
Copyright © 2016 The Society of Theoretical and Applied Mechanics
https://doi.org/10.1017/jmech.2016.62 Published online by Cambridge University Press

An increase in Kn number can be attributed to a decrease in the characteristic length of the microchannel or an increase in the mean free path of gas molecules. When Kn increases, the rarefaction effect starts dominating the flow field and flow at boundary slips. Karniadakis *et al*. reported that the slip flow situation reduces the surface friction and increases the volume flow rate, thus reducing the nonlinear pressure distribution [4]. Colin *et al*. used nitrogen and helium gasses in a silicon-based microchannel to investigate the increase in the mass flow rate by using an inlet/outlet pressure ratio and decrease in Kn number at the outlet [5]. Jang and Wereley fabricated microcavities next to microchannel devices, which were connected to conventional pressure sensors, through micromachining and experimentally analyzed the pressure distribution inside microchannels [6]. They reported nonlinear pressure distributions inside the gas flow microchannels. Moreover, they investigated the channel location associated with the maximum pressure deviation from the conventional linear assumption and determined that this location shifted downstream as the inlet/outlet pressure ratio increased. They also observed the effect of rarefaction, which reduces the nonlinear pressure distribution, on the microchannel flow.

An experimental technique, called pressure/temperature-sensitive paint (PSP/TSP), that entails using luminescent molecules to measure the surface pressure and temperature was first developed in 1980 [7]. Luminescent molecules change their luminescence intensity in the presence of oxygen molecules in the environment, a phenomenon known as oxygen quenching, and the intensity can be further calibrated as surface pressure with the assumption of Henry's and Dalton's laws. Moreover, the luminescence intensity is affected by the temperature variation in the environment; specifically, an increase in temperature results in a drop in intensity. This phenomenon is known as thermal quenching. The luminescent molecules are mixed with a polymer binder to prepare PSP sensor, which is sprayed on a model surface for measurements. An ultraviolet (UV) light-emitting diode (LED) is used as the excitation source, and a charge-coupled-device (CCD) camera with a long-pass optical filter is used to receive the luminescence signal during measurements. A luminescent image acquired under ambient conditions is used as a reference image, and images captured during calibration and measurement are normalized using this reference image to eliminate the nonuniformity engendered by lighting and paint. The intensity ratio of the images obtained from measurements can be further converted into pressure data during data reduction. This technique has been applied to microfluidics to retrieve the details of pressure/temperature profiles inside various microdevices such as microchannels and micronozzles [8-11]. The experimental results acquired through PSP/TSP measurements are consistent with those acquired through theoretical and numerical analyses conducted in a previous study [12]. The details of PSP/TSP and the combination of luminescent molecules and polymer binders can be found in [7].

2. EXPERIMENTAL

In this study, two microchannel devices with dissimilar aspect ratios were fabricated through soft lithography. Both microchannels were 5mm long, and they respectively measured 100 and 50μm in width and 45 and 50μm in height; moreover, their aspect ratios were 2 and 1, respectively. A straight microchannel design involving a rectangular cross-section was used to analyze the effect of rarefaction on the microchannel gas flow. Luminescent molecules of Pt(II) meso-Tetra (Pentafluorophenyl) Porphine, PtTFPP, were used as pressure probes for the measurement. PDMS was used as the polymer binder to ensure that the luminescent molecules remained in the microchannel during the experiments. The PSP sensor, PtTFPP/PDMS, can be spin-coated on a glass slide. A glass slide with a PSP sensor of PtTFPP/PDMS could be directly bonded to the PDMS microchannel as the microchannel ceiling. A fluorescent microscope (Olympus, BX51) integrated with a CCD camera (PCO 1600) was used to receive luminescent signals, and a 400nm UV LED was used for excitation during PSP measurements. The spatial resolution of the PSP measurements was 3.73μm per pixel, which was obtained by integrating the microscope with a 4X objective lens. A vacuum pump was used to drive the gas flow in the microchannel, and this pump was connected to the microchannel outlet. A vacuum tank was placed between the vacuum pump and the microchannel to stabilize the pressure. A mass flow controller (MKS, 1179A) was connected to the microchannel inlet and open to the ambient condition for monitoring the flow rate in the microchannel during the experiments. Two reservoirs were constructed at the microchannel inlet and outlet to provide a steady flow rate. These reservoirs were connected to two vacuum pressure transducers (MKS, 901P) for monitoring the pressure during measurements. The pressure reading acquired at these reservoirs also served the pressure read out during in-situ calibration. To improve the accuracy of PSP measurements, in-situ and pixel-by-pixel calibrations were applied during data processing. Figure 1 illustrates a schematic of the experimental setup. Figure 2 presents the calibration curves of the PSP sensor, PtTFPP/PDMS, with the reference condition considered as the ambient condition. High consistency was achieved during three separate calibrations.

3. RESULTS AND DISCUSSION

To investigate the effect of rarefaction on the microchannel gas flow, PSP-based pressure measurements were conducted using two microchannels with different aspect ratios. Tables 1 and 2 list the experimental conditions for the PSP measurements of the 100-μm-wide microchannel (R100-1 ~ R100-10). The Reynolds number varied from 391 to 3.4, whereas the Kn number at the outlet increased from 0.006 to 0.066. The pressure ratios in this experiment were controlled between

https://doi.org/10.1017/jmech.2016.62 Published online by Cambridge University Press

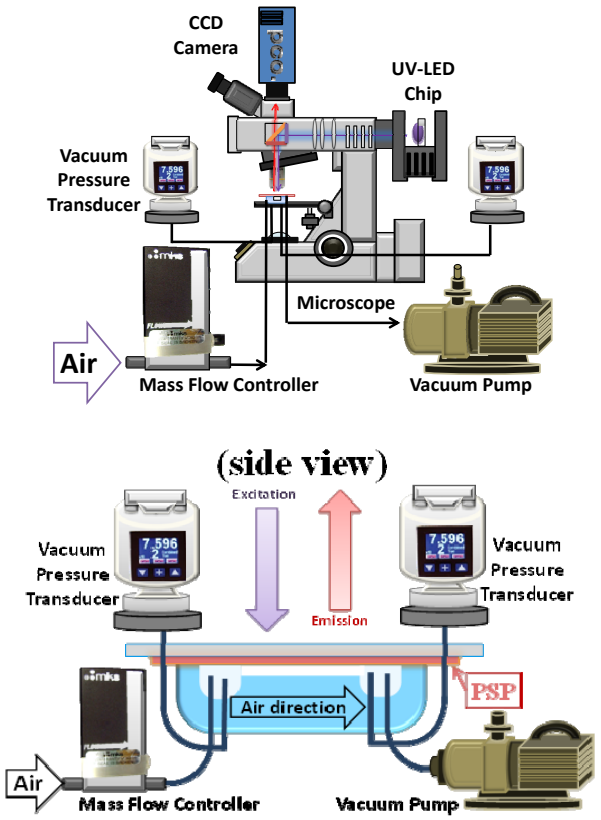


Fig. 1 Experimental setup of PSP measurements using a fluorescence microscope.

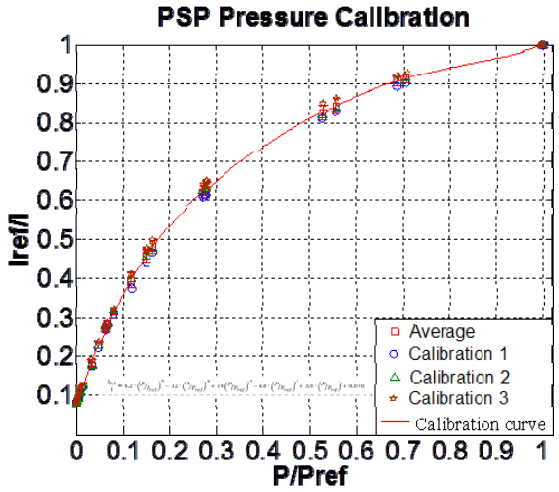


Fig. 2 Calibration curves of PSP sensor PtTFPP/PDMS.

2.9 and 5.4 to avoid the compressibility effect. Tables 3 and 4 list the experimental conditions for the PSP measurements of the 50-μm-wide microchannel (R50-1 ~ R50-11). The Reynolds number decreased from 217 to 0.82, whereas the Kn number at the outlet increased from 0.005 to 0.14. The pressure ratios in this experiment were controlled between 2.6 and 4 to separate the compressibility effect. Figure 3 presents detailed pressure maps acquired from the PSP measurements in R100-1 and R50-1. Certain regions were affected by the light reflected from the side wall, and these regions are masked as white strips along the side wall. The

Table 1 Experimental conditions of pressure measurements in a 100-μm-wide microchannel (Case R100-1 ~ R100-5).

	R100-1	R100-2	R100-3	R100-4	R100-5
Flow rate(sccm)	28.5	25	24	21.5	19
PSP inlet(kPa)	90.7	79.0	76.8	69.5	60.1
PSP outlet(kPa)	16.9	15.4	15.4	15.0	13.4
Pressure ratio	5.4	5.1	5.0	4.6	4.5
Mas flow rate Analytic (kg/s)	5.2e-07	3.9e-07	3.7e-07	3.0e-07	2.3e-07
Kni(inlet)	0.001	0.001	0.001	0.002	0.002
Kno(outlet)	0.006	0.007	0.007	0.007	0.008
Re	3.91e+02	2.69e+02	2.80e+02	2.28e+02	1.70e+02

Table 2 Experimental conditions of pressure measurements in a 100-μm-wide microchannel (Case R100-6 ~ R100-10).

	R100-6	R100-7	R100-8	R100-9	R100-10
Flow rate(sccm)	16	11.5	9	5.5	2.5
PSP inlet(kPa)	51.7	37.4	30.2	19.4	7.8
PSP outlet(kPa)	12.3	9.9	8.7	6.7	1.5
Pressure ratio	4.2	3.8	3.5	2.9	5.2
Mas flow rate Analytic (kg/s)	1.7e-07	8.7e-08	5.6e-08	2.3e-08	4.5e-09
Kni(inlet)	0.002	0.003	0.003	0.005	0.013
Kno(outlet)	0.008	0.010	0.012	0.015	0.066
Re	1.26e+02	6.53e+01	4.23e+01	1.69e+01	3.35e+00

luminescence signal along the side wall changed because of the trapezoidal cross-section of the microchannel; therefore, the pressure data, which were translated from the luminescence, were inaccurate and are masked to avoid confusion [13]. Figures 4(a) and 4(b) show the pressure distributions of R100-1 ~ R100-10 in the 100-μm-wide microchannel (x is the distance from the inlet and L is the microchannel length). Detailed pressure evolutions, along the centerline in the microchannel under various experimental conditions, were acquired through PSP measurements conducted from the inlet to the outlet of the microchannel. The nonlinear pressure distribution, which was clearly observed in R100-1, gradually decreased and flattened at R100-10. Figures 5(a) and 5(b) illustrate the dimensionless deviations of cases R100-1 ~ R100-10, which were calculated by subtracting the linear pressure gradient from the inlet to outlet and then dividing by the pressure difference between the inlet and the outlet. The highest dimensionless deviation of R100-1 was 0.25 and was located at x/L of 0.7 [Fig. 5(a)]. The maximum deviation of R100-6 was 0.05, and the peak was located at 0.6 [Fig. 5(b)]. The decrease in the pressure deviation from the linear assumption could be clearly observed, and the pressure evolution returned to a linear distribution once the Kn number (at the outlet) was greater than 0.012. Figures 6(a) and 6(b) present the pressure distributions along the centerline of the 50-μm-wide microchannel for R50-1 ~ R50-11. Fig-

https://doi.org/10.1017/jmech.2016.62 Published online by Cambridge University Press

ures 7(a) and 7(b) illustrate the dimensionless deviations for R50-1 ~ R50-11. The deviations from the linear distribution decreased from 0.15 (R50-1) to 0 (R50-11) as the outlet Kn number increased, similar to the 100-μm-wide microchannel. However, the maximum deviation of R50-1 was located between 0.5 and 0.8, and no peak was observed. Similar results were observed from the other measurements of the 50-μm-wide microchannel (R50-1 ~ R50-11), and no apparent peak could be identified from the corresponding pressure profiles. The degrees of nonlinearity (maximum deviation from linearity) of R100 and R50 were calculated and are plotted in Figs. 8(a) and 8(b), respectively. The nonlinearity of the 100-μm-wide microchannel decreased as the outlet Kn number increased; it was zero when the outlet Kn number was greater than 0.12. By contrast, the nonlinearity of the 50-μm-wide microchannel dropped gradually compared with that of the 100-μm-wide microchannel. The maximum deviation remained at approximately 0.02, whereas the outlet Kn number was greater than 0.14. Notably, even when the Reynolds numbers of these two cases (R100-8: Re = 42 and R50-9: Re = 24) were close, the nonlinearity was not diminished in the 50-μm-wide microchannel, and this is attributable to the narrowness of this microchannel, as indicated by its aspect ratio of 1.

Table 3 Experimental conditions of pressure measurements in a 50-μm-wide microchannel (Case R50-1 ~ R50-5).

Flow rate(sccm)	12.5	11	10	9	8.5
PSP inlet(kPa)	89.3	81.1	75.9	68.8	64.5
PSP outlet(kPa)	29.4	28.6	27.6	25.8	23.1
Pressure ratio	3.0	2.8	2.8	2.7	2.8
Mas flow rate Analytic (kg/s)	2.2e-07	1.8e-07	1.6e-07	1.3e-07	1.1e-07
Kni(inlet)	0.002	0.002	0.002	0.002	0.002
Kno(outlet)	0.005	0.005	0.005	0.006	0.006
Re	2.17e+02	1.76e+02	1.53e+02	1.24e+02	1.11e+02

Table 4 Experimental conditions of pressure measurements in a 50-μm-wide microchannel (Case R50-6 ~ R50-11).

	R50-6	R50-7	R50-8	R50-9	R50-10	R50-11
Flow rate(sccm)	7.5	6	5.5	4	3.5	0.9
PSP inlet(kPa)	55.5	46.7	41.3	29.4	24.0	4.8
PSP outlet(kPa)	20.8	17.5	16.0	10.7	8.2	1.2
Pressure ratio	2.7	2.7	2.6	2.8	2.9	4
Mas flow rate Analytic (kg/s)	8.7e-08	6.0e-08	4.6e-08	2.4e-08	1.7e-08	8.4e-10
Kni(inlet)	0.003	0.003	0.004	0.005	0.006	0.034
Kno(outlet)	0.007	0.008	0.009	0.014	0.018	0.140
Re	8.49e+01	5.81e+01	4.49e+01	2.36e+01	1.63e+01	8.21e-01

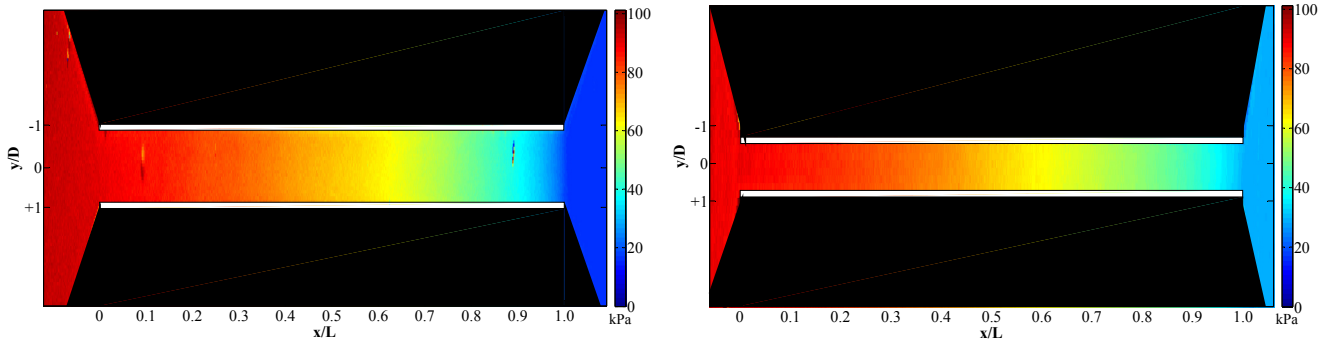


Fig. 3 Detailed pressure maps in (a) 100-μm-wide microchannel and (b) 50-μm-wide microchannel.

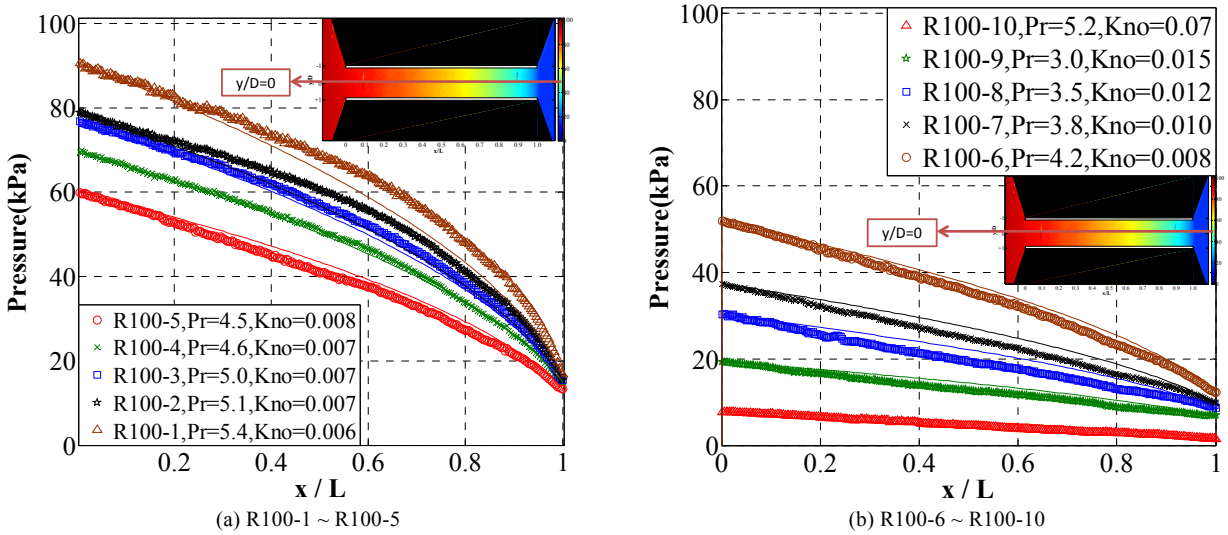
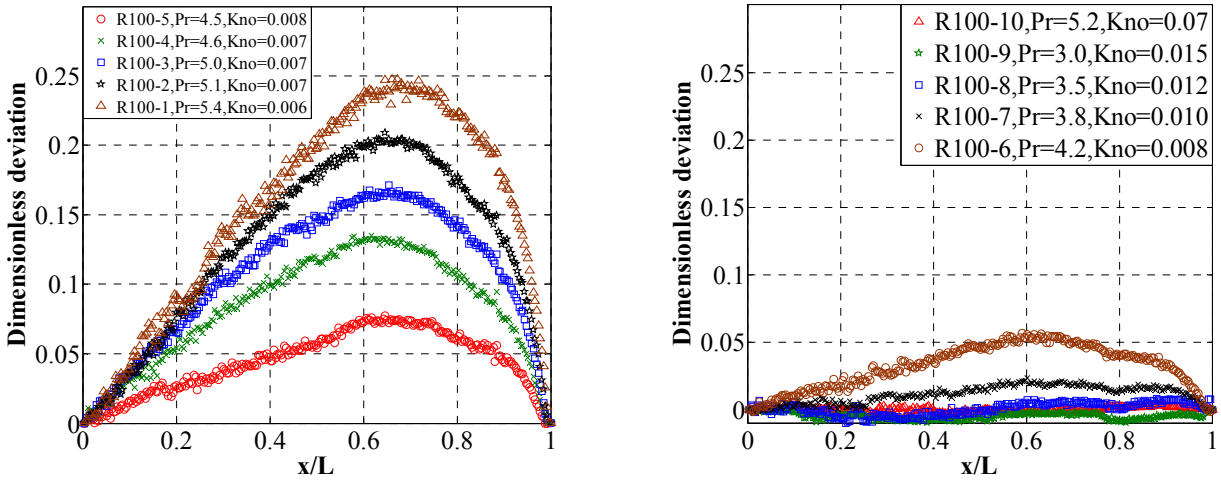


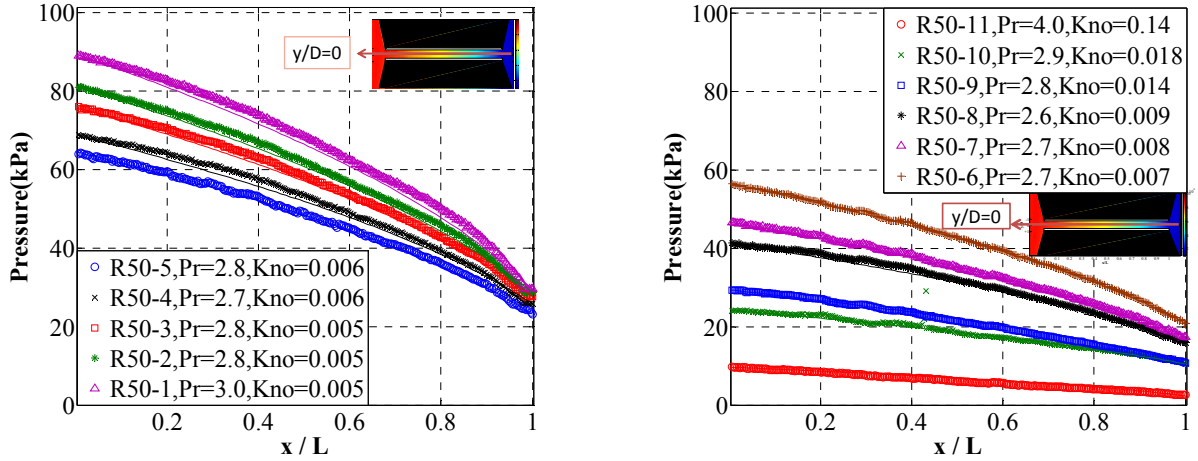
Fig. 4 Pressure distributions along the centerline inside a 100-μm-wide microchannel at different experimental conditions.

https://doi.org/10.1017/jmech.2016.62 Published online by Cambridge University Press



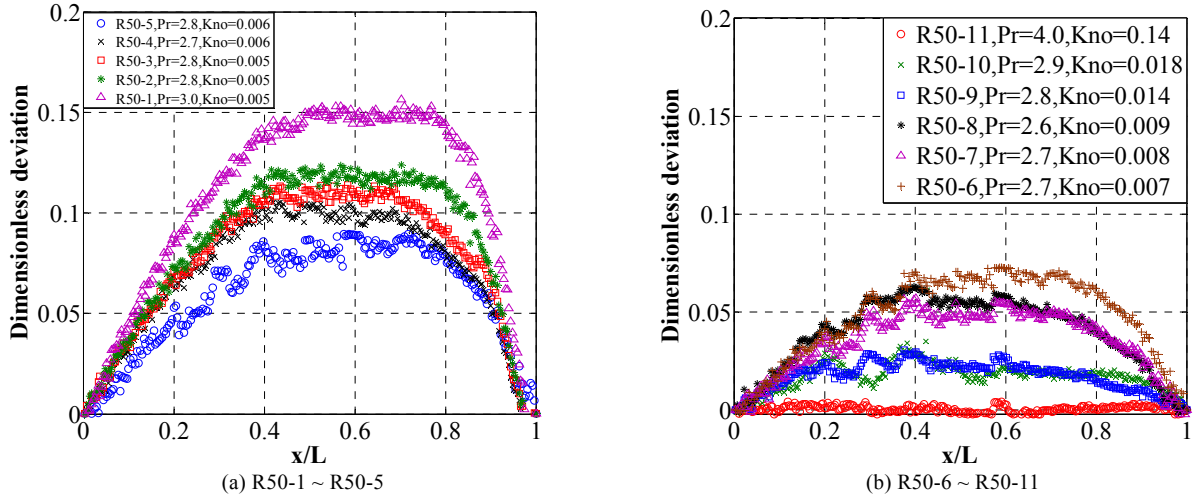
(a) R100-1~R100-5 (b) R100-6~R100-10

Fig. 5 Dimensionless deviations in a 100-μm-wide microchannel at different experimental conditions.



(a) R50-1~R50-5 (b) R50-6~R50-11

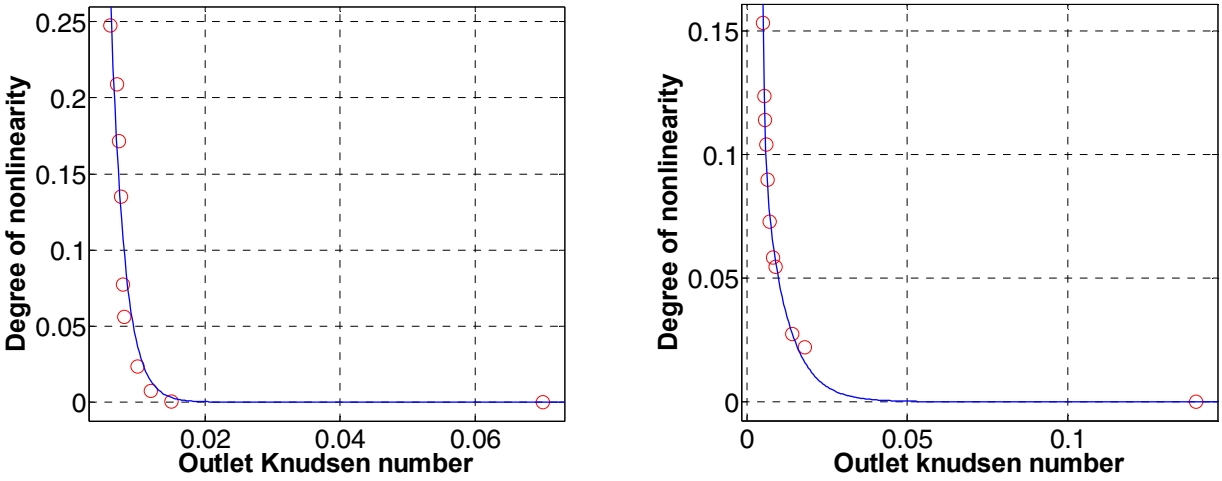
Fig. 6 Pressure distributions along the centerline inside a 50-μm-wide microchannel at different experimental conditions.



(a) R50-1 ~ R50-5 (b) R50-6 ~ R50-11

Fig. 7 Dimensionless deviations in a 50-μm-wide microchannel at different experimental conditions.

https://doi.org/10.1017/jmech.2016.62 Published online by Cambridge University Press



(a) 100-μm-wide microchannel (b) 50-μm-wide microchannel

Fig. 8 Degree of nonlinearity in (a) 100-μm-wide microchannel and (b) 50-μm-wide microchannel.

4. CONCLUSIONS

Detailed pressure distributions inside microchannels with different aspect ratios were effectively acquired through PSP, with the Kn number varying from 0.006 to 0.14, which is in the transitional flow regime (Kn > 0.1). The pressure evolutions from the inlet to the outlet were obtained, and the deviations from the linear assumption were analyzed. The drop in nonlinearity indicated by the pressure data as the outlet Kn number increased was clearly observed through the experimental data of R100 and R50. However, different behaviors were observed in the maximum deviations for R100 and R50; no apparent peak was observed for the pressure profiles of R50. The pressure data acquired in this study can be valuable for the design of a Knudsen pump, which uses a narrow microchannel to transport molecules.

ACKNOWLEDGEMENTS

This study was financially supported by the MOST project MOST 104-2221-E-007-102.

REFERENCES

1. Pong, K., Ho, C., Liu, J. and Tai, Y., "Non-Linear Pressure Distribution in Uniform Microchannels," *Application of Microfabrication to Fluid Mechanics*, **197**, pp. 51–51 (1994).
2. Arkilic, E. B., Schmidt, M. A. and Breuer, K. S., "Gaseous Slip Flow in Long Microchannels," *Journal of Microelectromech Systems*, **6**, pp. 167–178 (1997).
3. Hsieh, S. S., Tsai, H. H., Lin, C. Y., Huang, C. F. and Chien, C. M., "Gas Flow in a Long Microchannel," *International Journal Heat and Mass Transfer*, **47**, pp. 3877–3887 (2004).
4. Karniadakis, G. and Beskok, A., "Micro Flows: Fundamentals and Simulation," *Applied Mechanics Reviews*, **55**, p. 76 (2002).
5. Colin, S., Lalonde, P. and Caen, R., "Validation of a Second-Order Slip Flow Model in Rectangular Microchannels," *Heat Transfer Engineering*, 25, pp. 23–30, (2004).
6. Wereley, S. T. and Jang, J., "Pressure Distributions of Gaseous Slip Flow in Straight and Uniform Rectangular Microchannels," *Microfluid Nanofluid*, **1**, pp. 41–51 (2004).
7. Liu, T. and Sullivan, J. P., *Pressure and Temperature Sensitive Paints*, Springer-Verlag: Berlin (2004).
8. Huang, C., Gregory, J. and Sullivan, J., "Microchannel Pressure Measurements Using Molecular Sensors," *Journal of Microelectromech Systems*, **16**, pp. 777–785 (2007).
9. Huang, C., Gregory, J. and Sullivan, J., "Flow Visualization and Pressure Measurement in Micronozzles," *Journal of Visualization*, **10**, pp. 281–288 (2007).
10. Huang, C., Li, C., Wang, H. and Liou, T., "The Application of Temperature-Sensitive Paints for Surface and Fluid Temperature Measurements in Both Thermal Developing and Fully Developed Regions of a Microchannel," *Journal of Micromechanics and Microengineering*, **23**, 037001 (2013).
11. Huang, C. Y., Li, C. A., Huang, B. H. and Liou, T. M., "The Study of Temperature Rise in a 90-Degree Sharp Bend Microchannel Flow Under Constant Wall Temperature Condition," *Journal of Mechanics*, **30**, pp. 661–666 (2014).
12. Guo, X. H., Huang, C. Y., Alexeenko, A. and Sullivan, J., "Numerical and Experimental Study of Gas Flows in 2D and 3D Microchannels," *Journal of Micromechanics and Microengineering*, **18**, 025034, (2008).
13. Huang, C. Y. and Lai, C. M., "Pressure Measurements with Molecule-Based Pressure Sensors in Straight and Constricted PDMS Microchannels," *Journal of Micromechanics and Microengineering*, **22**, 065021 (2012).

(Manuscript received December 20, 2015, accepted for publication March 2, 2016.)

https://doi.org/10.1017/jmech.2016.62 Published online by Cambridge University Press